Published in final edited form as:
J Am Chem Soc. 2013 November 13; 135(45): 16758–16761. doi:10.1021/ja407438p.

A 2.8 Å Fe-Fe Separation in the $Fe_2^{III/IV}$ Intermediate (X) from Escherichia coli Ribonucleotide Reductase

Laura M. K. Dassama[1,2,&], **Alexey Silakov**[1], **Courtney M. Krest**[1,#], **Julio C. Calixto**[1], **Carsten Krebs**[1,2,*], **J. Martin Bollinger Jr.**[1,2,*], and **Michael T. Green**[1,*]

[1]Department of Chemistry, The Pennsylvania State University, University Park, Pennsylvania 16802, USA

[2]Department of Biochemistry and Molecular Biology, The Pennsylvania State University, University Park, Pennsylvania 16802, USA

Abstract

A class Ia ribonucleotide reductase (RNR) employs a μ-oxo-$Fe_2^{III/III}$/tyrosyl radical cofactor in its β subunit to oxidize a cysteine residue ~ 35 Å away in its α subunit; the resultant cysteine radical initiates substrate reduction. During self-assembly of the *Escherichia coli* RNR-β cofactor, reaction of the protein's $Fe_2^{II/II}$ complex with O_2 results in accumulation of an $Fe_2^{III/IV}$ cluster, termed **X**, which oxidizes the adjacent tyrosine (Y) 122 to the radical (Y_{122}•) as the cluster is converted to the μ-oxo-$Fe_2^{III/III}$ product. As the first high-valent non-heme-iron enzyme complex to be identified and the key activating intermediate of class Ia RNRs, **X** has been the focus of intensive efforts to determine its structure. Initial characterization by extended X-ray absorption fine structure (EXAFS) spectroscopy yielded a 2.5 Å Fe-Fe separation ($d_{Fe\text{-}Fe}$), which was interpreted to imply the presence of three single-atom bridges (O^{2-}, HO^-, and/or μ-1,1-carboxylates). This short $d_{Fe\text{-}Fe}$ has been irreconcilable with computational and synthetic models, which all have $d_{Fe\text{-}Fe} \geq 2.7$ Å. To resolve this conundrum, we revisited the EXAFS characterization of **X**. Assuming that samples containing increased concentrations of the intermediate would yield EXAFS data of improved quality, we applied our recently developed method of generating O_2 *in situ* from chlorite using the enzyme chlorite dismutase to prepare **X** at ~ 2.0 mM, > 2.5 times the concentration realized in the previous EXAFS study. The measured $d_{Fe\text{-}Fe}$ of 2.78 Å is fully consistent with computational models containing a $(\mu\text{-oxo})_2$-$Fe_2^{III/IV}$ core. The correction of $d_{Fe–Fe}$ brings the experimental data and computational models into full conformity and thus informs analysis of the mechanism by which **X** generates Y_{122}•.

Ribonucleotide reductases (RNRs) catalyze the conversion of ribonucleotides to deoxyribonucleotides, thus providing all organisms with precursors for the *de novo*

Corresponding Authors: mtg10@psu.edu, jmb21@psu.edu, ckrebs@psu.edu.
[&]Present address: Department of Molecular Biosciences, Northwestern University, Evanston, IL.
[#]Present address: Department of Chemistry, Stanford University, Stanford, CA.

ASSOCIATED CONTENT

Supporting Information. Method of sample preparation; Mössbauer spectra of the samples containing **X**, the reactant complex, and the product of decay of **X**; XANES spectra of the samples containing **X**, the reactant complex, and the product complex; XANES and EXAFS spectra of the second scans of samples containing **X**; additional presentations of fits to the EXAFS data; description of computational methodology and tables with results. This material is available free of charge via the Internet at http://pubs.acs.org

synthesis and repair of DNA.[1,2] All RNRs identified to date utilize a free-radical mechanism. A transient cysteine thiyl radical (C•),[3] generated *in situ* in the first step of the reaction, abstracts a hydrogen atom from the 3'-position of the bound nucleotide. The mechanism by which the C• is generated in each turnover is the basis for the division of RNRs into classes I-III.[1,2]

A class Ia RNR, such as the prototypical orthologue from aerobically-growing *Escherichia coli* (*Ec*), functions as a 1:1 complex of homodimeric subunits, α_2 and β_2. The α subunit binds substrates and allosteric effectors and contains the C residue (C_{439} in *Ec* RNR) that is oxidized to the C•, whereas the β subunit self-assembles a μ-oxo-$Fe_2^{III/III}$/tyrosyl radical cofactor that functions to generate the C• reversibly in each catalytic cycle.[4,5] The functional cofactor is produced by reaction of the $Fe_2^{II/II}$ complex of β with O_2.[6] Addition of O_2 yields a μ-peroxo-$Fe_2^{III/III}$ (**P**) complex[7–9] that is reduced upon cleavage of the O−O bond of the peroxo moiety. In the *Ec* β reaction, the O–O-cleavage step results in the one-electron oxidation of the solvent-accessible W_{48} to a cation radical (W_{48}^{+}•)[10] with concomitant formation of an $Fe_2^{III/IV}$ form of the diiron cluster termed cluster **X.**[11] The *Ec* W_{48}^{+}• can be reduced *in vitro* by small-molecule reductants including ascorbate and thiols,[10] but it is possible that an accessory protein serves as the reductant *in vivo*.[12] The decay of the W_{48}^{+}• leaves **X** to oxidize the nearby Y_{122} residue to the stable Y_{122}•. In the process, **X** is reduced to the μ-oxo-$Fe_2^{III/III}$ cluster of the active β subunit.[6,11,13] The Y• is strictly conserved among all class Ia and Ib RNRs and is absolutely required for their activity.[1,4,14]

The importance of **X** to the function of class Ia RNRs (which include the *Homo sapiens* orthologue) has made it a prime target for structural characterization. For *Ec* RNR, the rapid rate at which **X** decays (~ 1 s^{-1} in the wild type β; 0.2 s^{-1} in the Y_{122}F variant at 5 °C[11,13]) has thus far prevented characterization by X-ray crystallography. Instead, the freeze-quench technique has been used to trap the intermediate, and it has then been characterized by a variety of spectroscopic methods.[13,15–21] Density functional theory (DFT) calculations have afforded models for its diiron core, and these models have been evaluated for consistency with the spectroscopic data.[22–26] This approach, now commonplace in investigations of reactive metalloenzyme intermediates,[27] has thus far failed to forge a consensus regarding the structure of **X**. The primary reason is that the short Fe-Fe separation ($d_{Fe\text{-}Fe}$ ~ 2.5 Å)[19] of the intermediate determined by extended X-ray absorption fine structure (EXAFS) spectroscopy seemingly requires a structure with three single-atom bridges provided by some combination of the protein carboxylate ligands and O_2/solvent-derived hydr(oxo) ligands. Such a structure has been disfavored in computational studies on energetic grounds. Indeed, structures favored in these studies have values of $d_{Fe\text{-}Fe} \geq 2.7$ Å and no more than two single-atom oxygen bridges.[16,23–25] Furthermore, none of the available synthetic models for **X** has had such a short $d_{Fe\text{-}Fe}$.[28–30] Additionally, structural metrics determined by EXAFS for a Mn^{IV}/Fe^{III} homolog of **X** in the RNR from *Chlamydia trachomatis* have agreed with those derived by DFT, [31] indicating that current DFT methods are capable of accurately predicting the structures of such enzyme-bound dinuclear complexes.

We sought to resolve the conundrum concerning the structure of **X** by revisiting the irreconcilably short $d_{Fe\text{-}Fe}$ determined in the initial EXAFS study. The kinetics of the activation reaction preclude trapping of **X** in pure form, with a maximum fraction of ~ 0.7

having been achieved in published studies. The challenging kinetics had conspired with the poor solubility of O_2 in aqueous solutions (< 2 mM at 1 atm) to limit the concentration of **X** that could be trapped to < 0.8 mM. Recent technological advancements now permit accumulation of O_2-derived intermediates at concentrations exceeding 2 mM,[32] and we reasoned that the ability to trap **X** at elevated concentrations might yield samples of higher quality to permit the re-characterization of the intermediate by EXAFS.

Samples for this study were prepared by the method of generating O_2 *in situ* from chlorite (ClO_2^-) with the enzyme chlorite dismutase (Cld). A reactant solution containing a high concentration of the pre-formed $Fe_2^{II/II}$ complex of *Ec* RNR-β-Y_{122}F and a catalytic concentration (12.5 μM) of Cld was mixed with 0.25 equivalent volumes of a second reactant solution containing ClO_2^-, and the reaction was freeze-quenched after 0.3 s (at 5 °C). The 4.2-K/53-mT Mössbauer spectra of the freeze-quenched samples reveal the presence of ~ 65% **X**, comparable to the maximum fraction obtained in the previous EXAFS study, along with ~ 18 % unreacted Fe^{II} species and ~ 18 % of μ-oxo-$Fe_2^{III/III}$ product cluster (Figures S1-S3 of the Supporting Information). This fraction of **X** corresponds to 2.0 mM, more than 2.5 times the maximum concentration attained in the previous EXAFS study.

The X-ray absorption near-edge structure (XANES) spectra (Figure S4) show a higher K-edge absorption energy (the energy at which the 1s-core electron is ejected) for samples containing **X** than for the samples of the unreacted $Fe_2^{II/II}$-β starting material. However, the edge of the **X** samples lies at a *lower* energy than for samples of the μ-oxo-$Fe_2^{III/III}$ product. This phenomenon, also observed by Riggs-Gelasco et al.,[19] may result from the contribution of the unreacted $Fe_2^{II/II}$ component in the freeze-quenched samples of **X**. Alternatively, the skewing of the edge energy to a lower value may be a feature inherent to **X** that remains to be explained theoretically.

Fe K-edge EXAFS data over $k = 0.3 – 14$ Å^{-1} (for samples containing the $Fe_2^{II/II}$ reactant complex and the μ-oxo-$Fe_2^{III/III}$ product state) and $k = 0.3 – 16$ Å^{-1} (for samples containing **X**) are shown in Figure 1, along with fits to the raw data based on the parameters given in Tables 1 and S1-S3. The EXAFS data of the $Fe_2^{II/II}$ reactant complex (Figure 1A, left panel) are best fit with a model that contains a total coordination number of four oxygen/nitrogen (O/N) ligands per Fe. This value is consistent with the crystal structure of that enzyme form.[33] There is no evidence for an Fe-Fe scatterer in the Fourier transform (FT) of the EXAFS (Figure 1A, right panel), presumably because $d_{Fe\text{-}Fe}$ is too large (~ 3.8 Å[33]) in this form of the cluster. The EXAFS data of the μ-oxo-$Fe_2^{III/III}$ product cluster (Figure 1B, left panel) can be fit with a model that contains six O/N ligands per Fe.[34] Furthermore, the FT of the EXAFS data exhibits a prominent Fe scattering interaction at $R = 3.2$ Å (Figure 1B, right panel), a value that is also consistent with the reported $d_{Fe\text{-}Fe}$ of this form.[35,36]

The EXAFS data for the samples containing **X** (Figure 1C, left panel) can be fit by a model with 3 O/N at 2.01 Å, 2 O/N at 2.11 Å, and 0.65 O at 1.75 Å per Fe. This fit also includes two Fe-Fe scattering interactions: 0.65 Fe at 2.78 Å, and 0.18 Fe at 3.22 Å (Table S3). The occupancies of the two Fe-Fe scattering interactions account for the heterogeneity of the sample, specifically the fractions of **X** and μ-oxo-$Fe_2^{III/III}$ cluster determined from the

Mössbauer data. The contribution to the Fe-Fe scattering interactions in the EXAFS data from the ~ 18% $Fe_2^{II/II}$ component in the samples is not obvious and is not accounted for in the analysis. The Fe-O/N interaction at 1.75 Å is likely to arise from an oxo bridge, and the occupancy of 0.65 is consistent with the presence of *two* such μ-oxo interactions in an asymmetric di-μ-oxo-Fe_2 core (see Table S3 for additional fitting results).

The agreement between the fit and the data at $R \geq$ ~3.0 Å can be improved through the inclusion of additional non-nearest-neighbor scattering interactions. Examination of the crystal structures of the reactant and product complexes reveals the presence of carbon atoms from the bridging and terminal carboxylates and histidines that could contribute to scattering interactions at ~ 3.0 and ~ 3.2 Å. In the crystal structure of the $Fe_2^{III/III}$ product state (1RIB), there are a total of 6 carbons (three per Fe) at ~ 3.0 Å and 2 carbons (one per Fe) at 3.2 Å away from the Fe ions.[34] Assuming that these atoms might also be present at similar distances in the samples containing **X**, we included three Fe-C scattering interactions at 3.0 Å and one at 3.2 Å into the fit model. Their inclusion significantly improves the agreement between the fit and the data (Figure 1D; parameters provided in Table 1). It is unclear why these interactions would be required for fits of **X** but not the diferric EXAFS. It is possible that the high-valent **X** contains a tighter core, making these scattering interactions pronounced. Irrespective of the origin of the additional interactions, the dominant scattering interaction at ~2.8 Å can be assigned to an Fe scatterer, and there is no evidence for an interaction at the previously reported $d_{Fe\text{-}Fe}$ of ~ 2.5 Å.

To determine the structure of the diiron core of **X** and rationalize the 2.8 Å $d_{Fe\text{-}Fe}$, we generated a series of structural models by broken-symmetry DFT methods, following previous work by Noodleman and coworkers[22–26] (see Supporting Information for a more detailed description). The models were derived from the X-ray crystallographic data (1RIB) of *Ec* β by modifying the ligation. Two main candidates were examined in detail, a di-(μ-oxo)-(μ-1,3-carboxylato) core structure and a (μ-oxo)(μ-hydroxo)(μ-1,3-carboxylato) structure (Figure 2). The di-(μ-oxo) model has distance parameters that closely match the experimentally determined values, including, most notably, the $d_{Fe\text{-}Fe}$ of 2.8 Å (Figure 2).

It is noteworthy that the DFT calculations imply that protonation of one of the μ-oxo bridges should result in an elongation of the Fe-Fe separation to ~ 3.0 Å, the distance at which a minor scatterer is detectable in the data. The results of magnetic circular dichroism studies on **X** suggested a model in which one of the bridging oxo groups is protonated.[16] The inclusion of an Fe scatterer at ~3.0 Å (in lieu of additional C scatters at 3.0 and 3.2 Å) also improves the fit in this region. However, such a structure has remained inconsistent with data from ^{2}H-electron-nuclear double resonance experiments, which do not detect a bridging hydron.[18,20,21]

The effect of including the essential Y_{122} that is oxidized by **X** in the DFT calculations was also evaluated (see Supporting Information for a more detailed description of the computational methodology). Y_{122} forms a hydrogen bond to aspartate 84, which ligates Fe1 of the Fe−Fe cluster. Thus, its presence provides a proton transfer pathway by which one of the μ-oxo bridges in **X** might be protonated, thereby altering the core structure of the intermediate. The results of our DFT calculations, similar to those of Noodleman and co-

workers, show that the presence of Y_{122} has a minor effect on the optimized geometries, resulting in only a slight increase (~ 0.02 Å) in d_{Fe-Fe} (Table S9). Thus, it seems unlikely that the structure of **X** in the β-Y_{122}F variant could be significantly different from that formed in the wild-type protein.

In an effort to understand the basis for the discrepancy between the d_{Fe-Fe} of 2.8 Å determined here and the previously reported distance of 2.5 Å, we considered that third-generation synchrotron technology and the increased (2.5 ×) concentration of **X** (obtained through the use of Cld and ClO_2^-) could result in a critical increase in signal-to-noise ratio. Interestingly, this was not the case. The data from both studies have effectively the same signal-to-noise ratio. We also considered that the increased resolution provided by the extended *k*-range of our measurements might be critical to the observation of the 2.8 Å Fe-Fe distance. Whereas the data analyzed in the previous study were limited to $k = 2 – 12.6$ $Å^{-1}$, the data reported here were fit from $k = 0.3 – 16$ $Å^{-1}$. To evaluate whether this difference might be a plausible explanation for the discrepant results, we examined FTs of unfiltered EXAFS data with cutoffs at $k = 11$, 12, 13, 14, 15, and 16 $Å^{-1}$. Figure 3 shows that the intensity of the 2.8 Å peak does decrease with *k*, becoming a shoulder when $k_{max} = 11.0$ $Å^{-1}$. However, fits over five of the six *k* ranges listed in Figure 3 yield an Fe-Fe distance of 2.8 Å. (Fits of the shortest range, k=0–11 $Å^{-1}$, yield an Fe-Fe distance of 2.37 Å, with a large Debye-Waller factor of 0.01.) In no case does truncation of our data lead to the assignment of a 2.5 Å Fe-Fe scattering interaction. It appears then that the data reported herein and the previous study are inherently different, suggesting that they were obtained from inherently different samples (i.e., not from the same species). To illustrate this point, we overlay the EXAFS obtained from both studies in Figure S8.

This re-examination of the structure of **X** and subsequent upward adjustment of its d_{Fe-Fe} calls into question the short d_{Fe-Fe}s reported for other O_2-derived diiron intermediate complexes. For example, the high-valent $Fe_2^{IV/IV}$ complex, **Q**, that accumulates during the conversion of methane to methanol by the soluble methane monooxygenase from *Methylosinus trichosporium* OB3b was characterized by EXAFS, and the measured d_{Fe-Fe} of 2.46 Å led to the proposal of a [(μ-oxo)$_2$Fe$_2$] "diamond core" structure.[37] Subsequently, EXAFS characterization of the μ-peroxo-$Fe_2^{III/III}$ complexes that accumulate in the reactions of M ferritin from frog[38] and the $D_{84}E/W_{48}A$ variant of *Ec* RNR-β[39] led to reports of similar values of d_{Fe-Fe} (~ 2.5 Å) even in these mid-valent complexes. In general, the structures dictated by these surprisingly short Fe-Fe separations have been irreconcilable with synthetic and computational models, which predict d_{Fe-Fe}s of ~ 2.7 Å for **Q** and > 3.0 Å for the μ-peroxo-$Fe_2^{III/III}$ complexes.[40–43] Re-examination of these other complexes and re-determination of their Fe-Fe separations would seem to be warranted.

Supplementary Material

Refer to Web version on PubMed Central for supplementary material.

Acknowledgments

Portions of this research were carried out at the Stanford Synchrotron Radiation Lightsource, a Directorate of SLAC National Accelerator Laboratory and an Office of Science User Facility operated for the U.S. Department of

Energy Office of Science by Stanford University. The SSRL Structural Molecular Biology Program is supported by the DOE Office of Biological and Environmental Research, and by the National Institutes of Health, National Institute of General Medical Sciences (including P41GM103393). The authors thank beam line scientists Matthew J. Latimer and Erik J. Nelson for assistance during data acquisition.

Funding Sources

This work was supported by the National Institutes of Health (GM-55365 to JMB, CK, and MTG) and an Alfred P. Sloan Minority Ph.D. fellowship to LMKD.

ABBREVIATIONS

RNR	ribonucleotide reductase
Ec	*Escherichia coli*
DFT	Density Functional Theory
EXAFS	extended X-ray absorption fine structure
k	photoelectron wave vector
XANES	X-ray absorption near structure
FT	Fourier transform
BS	broken symmetry
COSMO	conductor-like screening model
ε	dielectric constant

REFERENCES

1. Nordlund P, Reichard P. Annu. Rev. Biochem. 2006; 75:681–706. [PubMed: 16756507]
2. Stubbe J. Curr. Opin. Struct. Biol. 2000; 10:731–736. [PubMed: 11114511]
3. Licht S, Gerfen GJ, Stubbe J. Science. 1996; 271:477–481. [PubMed: 8560260]
4. Stubbe J, Nocera DG, Yee CS, Chang MCY. Chem. Rev. 2003; 103:2167–2202. [PubMed: 12797828]
5. Stubbe J, Riggs-Gelasco P. Trends Biochem. Sci. 1998; 23:438–443. [PubMed: 9852763]
6. Atkin CL, Thelander L, Reichard P, Lang G. J. Biol. Chem. 1973; 248:7464–7472. [PubMed: 4355582]
7. Tong WH, Chen S, Lloyd SG, Edmondson DE, Huynh BH, Stubbe J. J. Am. Chem. Soc. 1996; 118:2107–2108.
8. Yun D, García-Serres R, Chicalese BM, An YH, Huynh BH, Bollinger JM Jr. Biochemistry. 2007; 46:1925–1932. [PubMed: 17256972]
9. Bollinger JM Jr, Krebs C, Vicol A, Chen S, Ley BA, Edmondson DE, Huynh BH. J. Am. Chem. Soc. 1998; 120:1094–1095.
10. Baldwin J, Krebs C, Ley BA, Edmondson DE, Huynh BH, Bollinger JM Jr. J. Am. Chem. Soc. 2000; 122:12195–12206.
11. Bollinger JM Jr, Edmondson DE, Huynh BH, Filley J, Norton JR, Stubbe J. Science. 1991; 253:292–298. [PubMed: 1650033]
12. Wu CH, Jiang W, Krebs C, Stubbe J. Biochemistry. 2007; 46:11577–11588. [PubMed: 17880186]
13. Ravi N, Bollinger JM Jr, Huynh BH, Edmondson DE, Stubbe J. J. Am. Chem. Soc. 1994; 116:8007–8014.
14. Stubbe J. Curr. Opin. Chem. Biol. 2003; 7:183–188. [PubMed: 12714050]

15. Mitić N, Saleh L, Schenk G, Bollinger JM Jr, Solomon EI. J. Am. Chem. Soc. 2003; 125:11200–11201. [PubMed: 16220933]
16. Mitić N, Clay MD, Saleh L, Bollinger JM Jr, Solomon EI. J. Am. Chem. Soc. 2007; 129:9049–9065. [PubMed: 17602477]
17. Sturgeon BE, Burdi D, Chen S, Huynh BH, Edmondson DE, Stubbe J, Hoffman BM. J. Am. Chem. Soc. 1996; 118:7551–7557.
18. Shanmugam M, Doan PE, Lees NS, Stubbe J, Hoffman BM. J. Am. Chem. Soc. 2009; 131:3370–3376. [PubMed: 19220056]
19. Riggs-Gelasco PJ, Shu L, Chen S, Burdi D, Huynh BH, Que L Jr, Stubbe J. J. Am. Chem. Soc. 1998; 120:849–860.
20. Burdi D, Sturgeon BE, Tong WH, Stubbe J, Hoffman BM. J. Am. Chem. Soc. 1996; 118:281–282.
21. Burdi D, Willems J-P, Riggs-Gelasco P, Antholine WE, Stubbe J, Hoffman BM. J. Am. Chem. Soc. 1998; 120:12910–12919.
22. Han W-G, Liu T, Lovell T, Noodleman L. J. Am. Chem. Soc. 2005; 127:15778–15790. [PubMed: 16277521]
23. Han W-G, Liu T, Lovell T, Noodleman L. J. Inorg. Biochem. 2006; 100:771–779. [PubMed: 16504298]
24. Han W-G, Liu T, Lovell T, Noodleman L. Inorg. Chem. 2006; 45:8533–8542. [PubMed: 17029364]
25. Han W-G, Noodleman L. Dalton Trans. 2009:6045–6057. [PubMed: 19623405]
26. Han W-G, Noodleman L. Theor. Chem. Acc. 2010; 125:305–317. [PubMed: 20445806]
27. Neese F. J. Biol. Inorg. Chem. 2006; 11:702–711. [PubMed: 16821037]
28. Zang Y, Dong Y, Que L Jr, Kauffmann K, Münck E. J. Am. Chem. Soc. 1995; 117:1169–1170.
29. Dong Y, Fujii H, Hendrich MP, Leising RA, Pan G, Randall CR, Wilkinson EC, Zang Y, Que L Jr, Fox BG, Kauffman K, Münck E. J. Am. Chem. Soc. 1995; 117:2778–2792.
30. Hsu H-F, Dong Y, Shu L, Young VG, Que L Jr. J. Am. Chem. Soc. 1999; 121:5230–5237.
31. Younker JM, Krest CM, Jiang W, Krebs C, Bollinger JM Jr, Green MT. J. Am. Chem. Soc. 2008; 130:15022–15027. [PubMed: 18937466]
32. Dassama LMK, Yosca TH, Conner DA, Lee MH, Blanc B, Streit BR, Green MT, DuBois JL, Krebs C, Bollinger JM Jr. Biochemistry. 2012; 51:1607–1616. [PubMed: 22304240]
33. Logan DT, Su X-D, Åberg A, Regnström K, Hajdu J, Eklund H, Nordlund P. Structure. 1996; 4:1053–1064. [PubMed: 8805591]
34. Nordlund P, Eklund H. J. Mol. Biol. 1993; 232:123–164. [PubMed: 8331655]
35. Scarrow RC, Maroney MJ, Palmer SM, Que L Jr, Salowe SP, Stubbe J. J. Am. Chem. Soc. 1986; 108:6832–6834.
36. Scarrow RC, Maroney MJ, Palmer SM, Que L Jr, Roe AL, Salowe SP, Stubbe J. J. Am. Chem. Soc. 1987; 109:7857–7864.
37. Shu L, Nesheim JC, Kauffmann KE, Münck E, Lipscomb JD, Que L Jr. Science. 1997; 275:515–518. [PubMed: 8999792]
38. Hwang J, Krebs C, Huynh BH, Edmondson DE, Theil EC, Penner-Hahn JE. Science. 2000; 287:122–125. [PubMed: 10615044]
39. Baldwin J, Krebs C, Saleh L, Stelling M, Huynh BH, Bollinger JM Jr, Riggs-Gelasco P. Biochemistry. 2003; 42:13269–13279. [PubMed: 14609338]
40. Gherman BF, Baik M-H, Lippard SJ, Friesner RA. J. Am. Chem. Soc. 2004; 126:2978–2990. [PubMed: 14995216]
41. Xue G, Wang D, De Hont R, Fiedler AT, Shan X, Münck E, Que L Jr. Proc. Natl. Acad. Sci. U.S.A. 2007; 104:20713–20718. [PubMed: 18093922]
42. Cranswick MA, Meier KK, Shan X, Stubna A, Kaizer J, Mehn MP, Münck E, Que L Jr. Inorg. Chem. 2012; 51:10417–10426. [PubMed: 22971084]
43. Han W-G, Noodleman L. Inorganica Chim Acta. 2008; 361:973–986. [PubMed: 19262682]

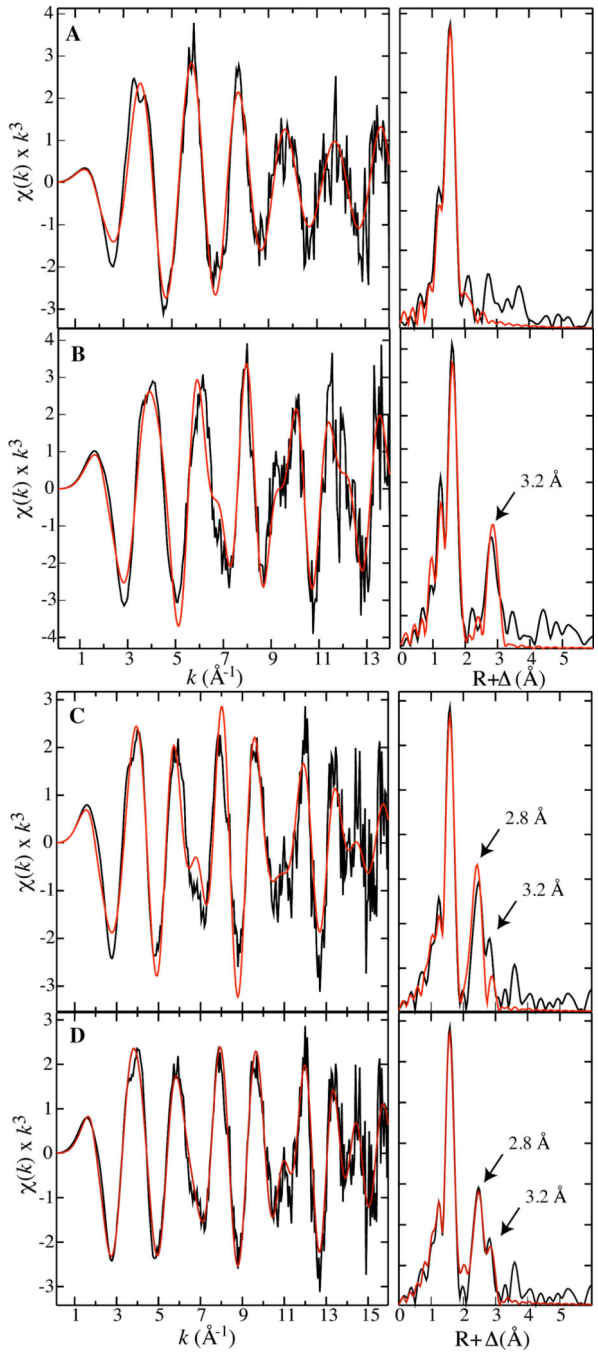

Figure 1.

Fe K-edge EXAFS data (left panel) and their Fourier transforms (right panel) for samples containing the $Fe_2^{II/II}$ reactant complex (**A**), the μ-oxo-$Fe_2^{III/III}$ product (**B**) and **X** (**C, D**). Fit parameters are provided in Tables 1, S1, S2, and S3.

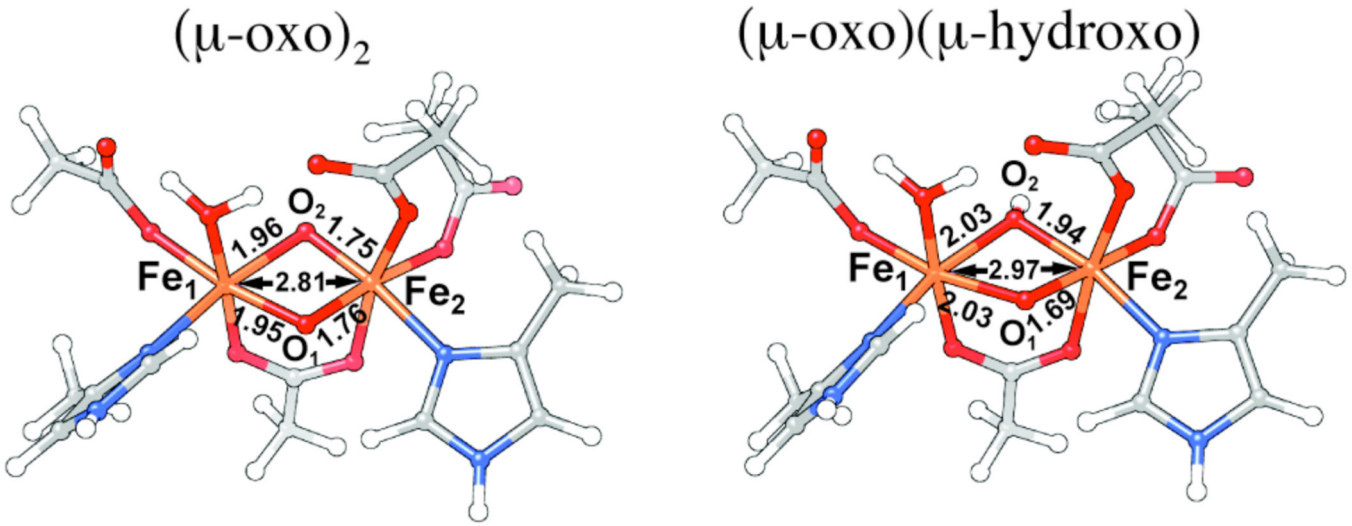

Figure 2.

Structural models for the $Fe_2^{III/IV}$ core of **X** derived from broken-symmetry DFT calculations. Left: $(\mu\text{-oxo})_2$ core; Right: (μ-oxo)(μ-hydroxo) core.

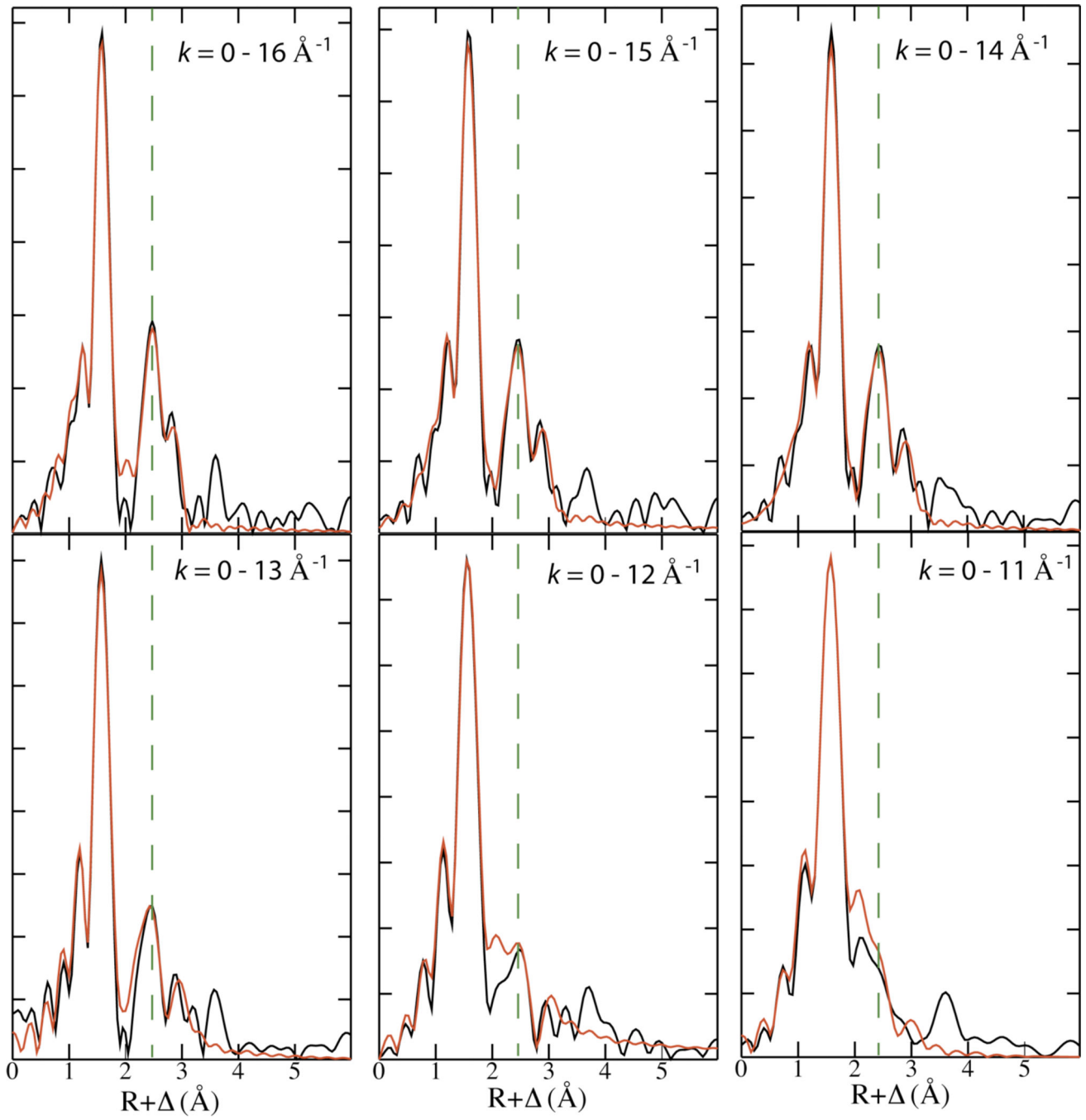

Figure 3.

FT of EXAFS data of samples containing **X** plotted with different cutoffs of the *k*-range. The dashed line is drawn at the middle of the ~ 2.8 Å peak. Overlaid in red is the FT resulting from the fit reported in Table 1.

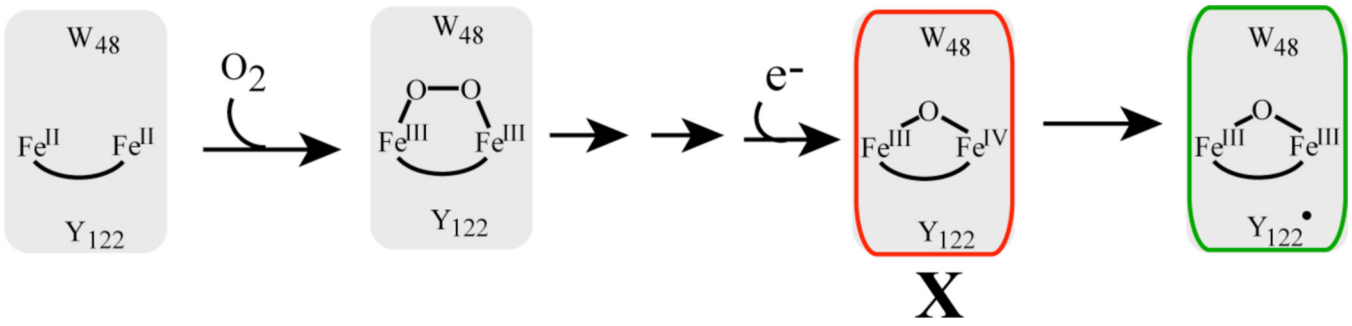

Scheme 1.

Schematic description of the activation Ec class Ia RNR. Intermediate **X** is the precursor to the active $Fe_2^{III/III}$/Y• cofactor.

Table 1

Fe K-edge EXAFS ($k = 0.3 - 16$ Å^{-1}) fitting results of samples containing **X** for which the fit model includes two discernable Fe−Fe interactions. Occupancies were fixed during the fit, but distances, Debye-Waller factors, and the threshold energy shift were allowed to vary

Scatterer Type	N	R	σ^2
Fe−O/N	5	2.02	0.0097
Fe−O	0.65	1.75	0.0020
Fe−C	3	2.97	0.0046
Fe−C	1	3.24	0.0060
Fe−Fe	0.65	2.79	0.0033
Fe−Fe*	0.18	3.22	0.0043
F	0.366		
$\mathbf{E_0}$	−11.067		
Resolution	0.099 Å		

N: occupancy; **R:** distance (Å); σ^2**:** Debye-Waller factor (Å^2); $\mathbf{E_0}$**:** threshold energy shift (eV); **F:** fit error.

*Parameters for this scattering interaction were constrained to the values obtained from fits of the diferric EXAFS